APPLICATION OF MARKOV-CHAIN MONTE CARLO PARAMETER-SET IDENTIFICATION TO DESIGN AND INVERSION

Sven M. Ivansson[a]

[a]SE-11529 Stockholm, Sweden

Sven M. Ivansson, SE-11529 Stockholm, Sweden; email sven.ivansson@gmail.com

Abstract: *In this paper, Markov-chain Monte Carlo (MCMC) sampling is used to identify sets in parameter space defined by the smallness of some "misfit" function. Two applications are given. The first concerns design of Alberich anechoic coatings with identification of coatings achieving a given maximum reflectance within a given frequency band. The layer-multiple-scattering (LMS) computational method is extended to cover three or more cavity types in the rubber coating. Three types turn out to improve the broad-band echo reduction, but no further improvement is obtained with four. Correlations among favourable design parameters are identified. The preferable cavity sizes typically increase with the rubber shear-wave velocity, but the smallest cavities are smaller than expected from a consideration of the resonance frequency of an isolated cavity. Effects of multiple scattering may explain this. The second application is about inversion uncertainty, with an example concerning determination of seismo-acoustic material parameters from backscattering measurements. With the a priori information that the difference between data and replica be within a certain error-norm bound, marginal estimates of the model parameters are computed. An interpretation is given in terms of Bayesian inversion with a certain simple data-error distribution, that does not involve additional data-error covariance parameters to be estimated.*

Keywords: *Anechoic coating, layer-multiple-scattering method, reflection/transmission matrix, Bayesian inversion*

1. INTRODUCTION AND SUMMARY

As detailed in [1], the Markov-chain Monte Carlo (MCMC) method, *e.g.*, [2], can be used to identify sets $G = \{\mathbf{p}: g(\mathbf{p}) < \varepsilon\}$, where $g(\cdot)$ is a computable function, in a space of parameter vectors $\mathbf{p}=(p_1,p_2,...)$. Volume-weighted projections of G onto parameter axes and two-dimensional parameter planes are thereby useful for visualization. An application to design of Alberich anechoic coatings was included in [1], using the layer-multiple-scattering (LMS) method [3],[4] for computation of the pertinent function $g(\cdot)$ defined as the maximum reflectance within a certain frequency band. Specifically, the coated structure was viewed as a phononic crystal (PC) slab for which the LMS method provided reflection/transmission (R/T) matrices for plane waves. The rubber-layer coatings contained long cylinder cavities of $S = 2$ sizes, with axes in a lateral direction.

The present paper includes an extension of this coating application to cavities of $S = 3$, or more, sizes. Secton 2 gives the details of the needed extension of the LMS method, and Sec. 3 provides coating-design results. The third cavity size improves the broad-band performance, but there is no further improvement with $S = 4$. As expected, for favourable coatings with $S = 3$, the sizes of the largest and medium cavities are positively correlated with the rubber shear speed. For the smallest cavities, however, there is a negative correlation, and they are much smaller than expected from a consideration of single-cavity resonances. This appears to be due to multiple scattering among the coating-layer cavities.

The MCMC identification of parameter sets can also be useful for assessment of inversion uncertainty. Section 4 gives an example, based on [5], concerning determination of seismo-acoustic material parameters from backscattering measurements in a water tank. Parameter values compatible with the measurements are identified. The approach can be reformulated in a Bayesian context, with a particularly simple data-error distribution. Sharper uncertainty estimates might result by using additional knowledge about the data errors, but estimation of additional data-error covariance parameters is avoided.

2. R/T MATRICES FOR A PC SLAB

The LMS method for computing R/T matrices for a PC slab with infinite cylindrical scatterers, detailed in [6], [7, Sec. III], and [1, Sec. III.C], is here extended to an arbitrary number S of scatterers within the unit cell of length d. In a Cartesian xyz coordinate system for position vectors $\mathbf{r} = (x,y,z)$, the cylinder axes are parallel to the y-axis, and cylinders of type σ=1,2,..,S appear at $\mathbf{r}_\sigma + \mathbf{R}$ where $\mathbf{r}_\sigma = (x_\sigma,0,0)$ and $\mathbf{R} = m(d,0,0)$ with m running through the integers. Figure 1 shows a coating example with $S = 3$.

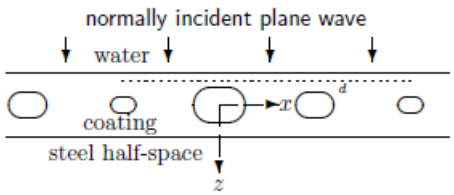

Fig.1: Coating containing cylindrical scatterers of three sizes between a steel and a water half-space. The medium is independent of y and periodic with period d in x.

The angular frequency of an insonifying plane wave is $\omega > 0$. At first, the scatterers are in an otherwise homogeneous anelastic solid whole-space with wavenumbers k_p and k_s for sound and shear waves, respectively, and with basic cylindrical displacement-vector

solutions $\mathbf{u}_{l\kappa}^{0P}(\mathbf{r})$ and $\mathbf{u}_{l\kappa}^{+P}(\mathbf{r})$ for regular (involving J_l) and outgoing (involving $H_l^{(1)}$) waves, respectively, as defined in [6]. P=L,M,N indicates wave type, l=0,±1,±2,.. angular order, and the real number κ controls the exp(iκy) dependence on y. $T_\sigma = \{(T_\sigma)_{l;l'}^{PP'}\}$ is the transition (T) matrix for a scatterer of type σ located at the origin. For a scatterer of type σ at $\mathbf{r}_\sigma$+$\mathbf{R}$, exp[i$\mathbf{k}_\parallel$·($\mathbf{r}_\sigma$+$\mathbf{R}$)] $\mathbf{b}_\sigma^+$ gives the expansion coefficients for its scattered field in terms of $\mathbf{u}_{l\kappa}^{+P}(\mathbf{r}-\mathbf{r}_\sigma-\mathbf{R})$, and exp[i$\mathbf{k}_\parallel$·($\mathbf{r}_j$+$\mathbf{R}$)] $\mathbf{b}_{\sigma\nu}^0$ gives the expansion coefficients for the scattered field from all other scatterers of type ν in terms of $\mathbf{u}_{l\kappa}^{0P}(\mathbf{r}-\mathbf{r}_\sigma-\mathbf{R})$. For σ=1,2,..,S,

$$\mathbf{b}_\sigma^+ = T_\sigma \cdot (\mathbf{a}_0 + \textstyle\sum_{\nu=1}^{S} \mathbf{b}_{\sigma\nu}^0)\ . \tag{1}$$

Here, $\mathbf{a}_0 = \{(a_0)_{l\kappa}^{0P}\}$ gives the coefficients for expansion of the incident plane wave with horizontal wavenumber $\mathbf{k}_\parallel = (k_{\parallel x},\kappa,0)$ in regular waves $\mathbf{u}_{l\kappa}^{0P}(\mathbf{r})$. Equation (1) gives the following linear equation system for determination of the $\mathbf{b}_\sigma^+ = \{(b_\sigma^+)_l^P\}$, σ=1,2,..,S:

$$\mathbf{b}_\sigma^+ = T_\sigma \cdot \left(\mathbf{a}_0 + \Omega^0 \cdot \mathbf{b}_\sigma^+ + \textstyle\sum_{\nu=1,\nu\neq\sigma}^{S} Q_{\sigma\nu} \cdot \mathbf{b}_\nu^+\right)\ . \tag{2}$$

Here, Ω^0 and $Q_{\sigma\nu}$ are lattice translation matrices such that $\mathbf{b}_{\sigma\sigma}^0 = \Omega^0 \cdot \mathbf{b}_\sigma^+$ and $\mathbf{b}_{\sigma\nu}^0 = Q_{\sigma\nu} \cdot \mathbf{b}_\nu^+$ for $\nu \neq \sigma$. With $p = \left(k_p^2 - \kappa^2\right)^{1/2}$, $q = (k_s^2 - \kappa^2)^{1/2}$, and $\nu \neq \sigma$, their nonzero elements are

$$\begin{aligned}
&(\Omega^0)_{l;l'}^{LL} = \Theta_{l-l'}(0; k_{||x}d, pd) \qquad (\Omega^0)_{l;l'}^{MM} = (\Omega^0)_{l;l'}^{NN} = \Theta_{l-l'}(0; k_{||x}d, qd)\\
&(Q_{\sigma\nu})_{l;l'}^{LL} = \Theta_{l-l'}\left((x_\nu - x_\sigma)/d; k_{||x}d, pd\right)\\
&(Q_{\sigma\nu})_{l;l'}^{MM} = (Q_{\sigma\nu})_{l;l'}^{NN} = \Theta_{l-l'}\left((x_\nu - x_\sigma)/d; k_{||x}d, qd\right)
\end{aligned} \tag{3}$$

where, for the dependence exp(−iωt) on time t, Im(p),Im(q) > 0 and, with sgn(0) = 0,

$$\Theta_l(x; k_{||x}d, kd) = \textstyle\sum_m \left(\frac{\mathrm{sgn}(x+m)}{\mathrm{i}}\right)^l \exp\left(\mathrm{i}k_{||x}d(x+m)\right) \mathrm{H}_l^{(1)}(kd|x+m|)\ . \tag{4}$$

Equations (3) follow from the Graf addition theorem for Bessel functions, expressed as

$$\mathrm{H}_l^{(1)}(kr_{x+m})\mathrm{e}^{\mathrm{i}l\theta_{x+m}} = \textstyle\sum_n \mathrm{H}_{l-n}^{(1)}(kd|x+m|)\left(\frac{\mathrm{sgn}(x+m)}{\mathrm{i}}\right)^{l-n} \mathrm{J}_n(kr)\mathrm{e}^{\mathrm{i}n\theta} \tag{5}$$

for integers l and m, complex nonvanishing k with Im(k) > 0, and polar coordinate representations r(sin(θ),cos(θ)) = r_{x+m}(sin(θ_{x+m}),cos(θ_{x+m})) + (d(x+m),0) with $r < d\ |x+m|$.

Using [6, Eq. (12)], essentially the Poisson summation formula, the total scattered field $\mathbf{u}_{\mathrm{sc}}(\mathbf{r}) = \sum_{\sigma=1}^{S}\sum_{Pl}(b_\sigma^+)_l^P \sum_{\mathbf{R}} \exp\left(i\mathbf{k}_{||}\cdot(\mathbf{r}_\sigma+\mathbf{R})\right)\mathbf{u}_{l\kappa}^{+P}(\mathbf{r}-\mathbf{r}_\sigma-\mathbf{R})$ can be expressed in terms of plane waves of different types P,SV,SH (j_{sc}=1,2,3, respectively), directions along the z-axis (s_{sc}=+/− for positive/negative), and horizontal wavenumbers $\mathbf{k}_\parallel$ + (2πm_{sc}/d,0,0), where m_{sc} runs over the integers. This provides the desired plane-wave R/T matrices, but incident plane waves for all j_{inc}=1,2,3, s_{inc}=+/−, and integers m_{inc} must be considered. For a PC slab with several scatterer or layer interfaces, parallel to the xy-plane, R/T matrices for the different interfaces can be combined recursively to form a total R/T matrix, *e.g.*, [4].

The matrices Ω^0 are independent of m_{inc}, where $\mathbf{k}_\parallel$ + (2πm_{inc}/d,0,0) is the horizontal wavenumber of the incident plane wave, while (for each m_{inc}) the matrices $Q_{\sigma\nu}$ depend on σ and ν only through $x_\nu - x_\sigma$. For the special case with uniform scatterer location according to x_σ = (σ−1)d/S, σ = 1,..,S, Eqs. (3)-(4) show that $Q_{\sigma\nu} = Q_{1\,\nu+1-\sigma}$ if $\sigma < \nu$, $Q_{\sigma\nu} = Q_{1\,\nu+1+S-\sigma}$ if $\nu < \sigma$, $Q_{\sigma\nu}$ is periodic with period S in m_{inc} which can be used to treat the

different m_{inc} in an order that minimizes the needed updates of the $Q_{\sigma\nu}$, and that $\Omega^0 + Q_{1\,2} + Q_{1\,3} + .. + Q_{1\,S} = \Omega^0_S$ where Ω^0_S is "the Ω^0 computed with d replaced by d/S" (Ω^0_S is of course periodic with period S in m_{inc}, but it is not independent of m_{inc}). For the special case when $k_{\|x} = 0$, $(\Omega^0)^{PP'}_{l;l'}$ vanishes if $l - l'$ is odd, "$(Q_{\sigma\nu})^{PP'}_{l;l'}$ computed for m_{inc}" = $(-1)^{l-l'}$ "$(Q_{\nu\sigma})^{PP'}_{l;l'}$ computed for $-m_{\text{inc}}$", and $(Q_{\sigma\nu})^{PP'}_{l;l'}$ vanishes if $|x_\nu - x_\sigma| = d/2$, m_{inc} is even, and $l - l'$ is odd. These observations are helpful to reduce the computational work.

Finally, a comment about the case when the scatterers of type σ=1,2,..,S get displaced an amount ζ_σ in the z-axis direction relative to the wave center used for computation of their T-matrices T_σ. The equation system (2) is then modified to

$$[S(\zeta_\sigma)]^{\mathrm{T}} \cdot \mathbf{b}^+_\sigma = T_\sigma \cdot [S(\zeta_\sigma)]^{\mathrm{T}} \cdot \left(\mathbf{a}_0 + \Omega^0 \cdot \mathbf{b}^+_\sigma + \textstyle\sum_{\nu=1,\nu\neq\sigma}^{S} Q_{\sigma\nu} \cdot \mathbf{b}^+_\nu\right) \qquad (6)$$

where the orthogonal matrices $S(\zeta)$ are defined as in [1, Sec. III.C]. It is appropriate in this case to introduce new "effective" lattice translation matrices $[S(\zeta_\sigma)]^{\mathrm{T}} \cdot \Omega^0 = \Omega^0 \cdot [S(\zeta_\sigma)]^{\mathrm{T}}$ and $[S(\zeta_\sigma)]^{\mathrm{T}} \cdot Q_{\sigma\nu} = Q_{\sigma\nu} \cdot [S(\zeta_\sigma)]^{\mathrm{T}}$, with elements that depend on l, l' through the difference $l - l'$ only, *cf.* [1, Sec. III.C].

3. COATING DESIGN

A coating design example from [1] is here modified to $S = 3$ uniformly located cavity types, as in Fig. 1. The steel parameters are 5850 and 3230 m/s for the sound and shear-wave speeds, respectively, and 7.7 kg/dm^3 for the density. The water sound speed is 1480 m/s. Each cylindrical cavity has a superelliptical cross section with symmetry half-axes of lengths a and b in the z- and x-directions, respectively. A coating with small reflectance in the frequency band 8-22 kHz is desired. At first, a vector $\mathbf{p}$ with six design parameters, $\mathbf{p} = (p_1,p_2,p_3,p_{3x},p_4,p_5)$ is varied, by differential evolution, to minimize the maximum reflectance in the band. The parameters are, with their variation intervals in brackets: Lattice period $p_1 = d$ [4-160 mm], coating thickness $p_2 = H$ [1-12 mm], length-scale quotient between the medium-sized and largest cavities p_3 [0.15-1.0], length-scale quotient between the smallest and medium-sized cavities p_{3x} [0.15-1.0] cavity excentricity parameter $p_4 = a/b$ [0.4-1.0], and rubber shear-wave speed $p_5 = \beta$ [60-400 m/s]. All cavities appear in the middle of the coating. The largest, medium-sized, and smallest ones have half-axes a_1, $a_2 = p_3\, a_1$, and $a_3 = p_{3x}\, a_2$, respectively, in the z-axis direction. The rubber compressional-wave absorption is, in each case, set to the lowest value consistent with the physical constraint for the bulk modulus. In this initial optimization, the rubber shear-wave absorption is 25 dB/wavelength, while the sound speed and density of the rubber agree with those of the water.

The lowest curve (at 15 kHz) in left panel of Fig. 2 shows the reflectance at optimum, with maximum −38.6 dB in the 8-22 kHz band. The other two curves, with larger reflectance maxima, concern $S = 1$ and 2. Extension to $S = 4$ did not improve the $S = 3$ result.

Next, the design parameter space is extended with rubber shear-wave absorption $p_6 = \delta$ [1-25 dB/wavelength], sound speed $p_7 = \alpha$ [1400-1600 m/s], and density $p_8 = \rho$ [0.9-1.3 kg/dm^3]. Moreover, with $S = 3$ cavity types, a simple variable transformation, *cf.* [1, Secs. II.C and IV.A], is applied to replace the parameters p_2,p_3,p_{3x} with the cylinder-size parameters a_1,a_2,a_3. The MCMC sampling method is used to identify the set G' in the extended and modified design space for which the 8-22 kHz band reflectance falls below −30 dB. The right panel of Fig. 2 shows projections of G' onto the β-a_1, β-a_2, β-a_3 planes. As expected [1, Sec. IV.A], β-a_1 as well as β-a_2 are positively correlated, and the corresponding contours mainly appear between the indicated $\omega a/\beta = 0.3$ lines, at 8 kHz

(upper line) and 22 kHz (lower line), for approximate single-cavity absorption cross-section maxima. Surprisingly, however, the β-a_3 contours mainly fall below the $\omega a/\beta = 0.3$ line for 22 kHz, and they indicate a negative correlation between β and a_3. The reason appears to be complicated effects of multiple scattering among the cavities. The three ring symbols in the figure indicate β, a_1, a_2, a_3 values at the optimum (for $S = 3$) from the left panel. With a much larger a_3 value, the three plus symbols indicate corresponding values for an optimization done by artificially ignoring multiple scattering among the cavities (setting pertinent Ω^0 and $Q_{\sigma\nu}$ from Sec. 2 to zero matrices).

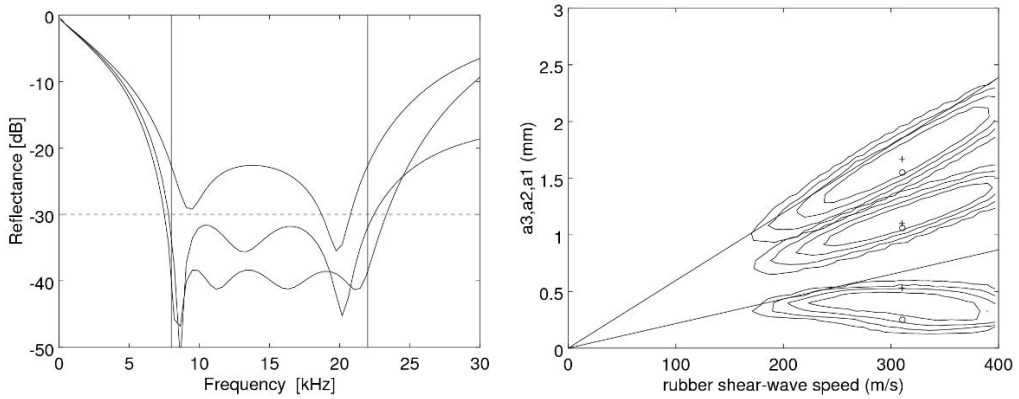

Fig.2: Left panel: reflectance curves obtained by minimizing the maximum reflectance in the indicated 8-22 kHz band; there are three curves, with improving results, for S = 1,2,3, respectively. Right panel: projections onto the β-a_1, β-a_2, β-a_3 planes of the set G′ with favourable coatings; for each of a_1, a_2, a_3, there are four contours enclosing minimal regions including 65%, 85%, 95%, and 99%, respectively, of the coatings in G′.

Further projections of G' (not shown) demonstrate that, for the favourable coatings: the lattice period d is concentrated around 50 mm; the excentricity parameter a/b appears in the interval (0.5,0.6) and it is negatively correlated with β, a_1, and a_2; the rubber shear-wave absorption δ is greater than 20 dB, while the reflectance is rather insensitive to the considered values of the negatively correlated rubber parameters α and ρ.

4. INVERSION UNCERTAINTY

Suppose that a data vector **d** has been obtained from some measurements, and consider the inverse problem to determine an underlying model parameter vector **p**. Without any errors, $\mathbf{d} = g_0(\mathbf{p})$ would hold, for a known computable forward-model function g_0. If an error-limit norm $\|\cdot\|$ with an error limit ε is also known, such that $\|\mathbf{d} - g_0(\mathbf{p})\| < \varepsilon$, the inversion uncertainty can be assessed by using MCMC sampling to identify the model set $G = \{\mathbf{p}: \|\mathbf{d} - g_0(\mathbf{p})\| < \varepsilon\}$.

Figure 12a in [5] shows a time trace, **d**, obtained by backscattering from a resin solid sphere in a certain tank-measurement configuration, devised to allow inversion of the resin parameters p_1 (compressional-wave speed), p_2 (shear-wave speed), p_3 (compressional-wave absorption), p_4 (shear-wave absorption). With the maximum norm and $\varepsilon = 4$ % (2 %) of the time-trace maximum, the solid (dashed) curves in Fig. 3 are histograms of volume-weighted projections of the corresponding set G onto the parameter axes. Such histograms can be useful for assessing inversion uncertainty and for designing measurement setups.

Finally a comment on the relation to Bayesian inversion. With standard notation, *e.g.*, [2], $P(\mathbf{p}|\mathbf{d}) \sim P(\mathbf{d}|\mathbf{p})\ P(\mathbf{p})$ according to Bayes' rule. With a uniform prior distribution $P(\mathbf{p})$ and with $P(\mathbf{d}|\mathbf{p}) \sim \exp(-E(\mathbf{p}))$ with the error or misfit function $E(\mathbf{p}) = 0$ when **p** is in $G = \{\mathbf{p}: \|\mathbf{d} - g_0(\mathbf{p})\| < \varepsilon\}$ and $+\infty$ when it is not, it follows that $P(\mathbf{p}|\mathbf{d}) \sim \chi_G(\mathbf{p})$, the characteristic

function of the set *G*. In Bayesian terminology, the projections in Fig. 3 of *G* onto the parameter axes are one-dimensional marginal posterior probability distributions.

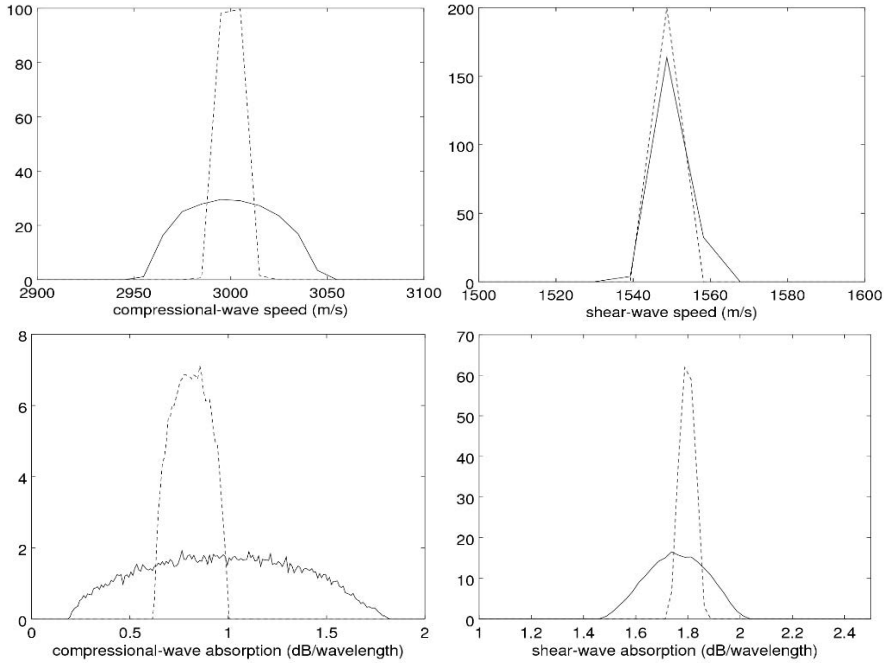

Fig.3: Histograms of projections onto the parameter axes of a set G of resin-parameter models compatible with certain backscatter measurements. The solid and dashed histograms concern different data-error limits, with halved limits for the dashed ones.

5. ACKNOWLEDGEMENTS

This work builds on experience gained while the author was with the Swedish Defence Research Agency. Stan Dosso provided one of his subroutines for MCMC model sampling.

REFERENCES

[1] **S.M. Ivansson**, Markov-chain Monte Carlo identification of favourable design choices with application to anechoic coatings, *J. Acoust. Soc. Am.*, 135 (6), pp. 3338-3351, 2014.
[2] **S.E. Dosso,** Quantifying uncertainty in geoacoustic inversion. I. A fast Gibbs sampler approach, *J. Acoust. Soc. Am.*, 111 (1), pp. 129-142, 2002.
[3] **R. Sainidou, N. Stefanou, I.E. Psarobas, A. Modinos**, A layer-multiple-scattering method for phononic crystals and heterostructures of such, *Comput. Phys. Commun.*, 166, pp. 197-240, 2005.
[4] **J.B. Pendry**, *Low Energ Electron Diffraction*, Academic Press, 1974.
[5] **A. Tesei, P. Guerrini, M. Zampolli**, Tank measurements of scattering from a resin-filled fiberglass spherical shell with internal flaws, *J. Acoust. Soc. Am.*, 124 (2), pp. 827-840, 2008.
[6] **S.M. Ivansson**, Designing 2D phononic crystal slabs with transmission gaps for solid angle as well as frequency variation, *Adv. Acoust. Vib.*, 2009, 317890, 2009.
[7] **S.M. Ivansson**, Anechoic coatings obtained from two- and three-dimensional monopole resonance diffraction gratings, *J. Acoust. Soc. Am.*, 131 (4), pp. 2622-2637, 2012.